Electronic Supplementary Information

Supra-amphiphile formed by complexation of azulene-based amphiphiles and pyrene in aqueous solution: from cylindrical micelles to disklike nanosheets

Fei Li, Qiao Song, Liulin Yang, Guanglu Wu, and Xi Zhang*

Key Lab of Organic Optoelectronics & Molecular Engineering Department of Chemistry, Tsinghua University, Haidian District,Beijing 100084, China.

Corresponding author: E-mail: xi@mail.tsinghua.edu.cn

Experimental section

NMR spectra were measured using JOEL JNM-ECA300 and JOEL JNM-ECA600 spectrometers; ESI-MS were recorded on a PE Sciex API 3000 spectrometer. UV-vis spectra were measured using a Hitachi U-3010 spectrophotometer; fluorescence spectra were measured using a Hitachi F-7000 apparatus. Unless otherwise noted, excitation and emission slits were 5.0 nm, and the scanning rate was 240 nm/min. TEM images were measured using a JEM 2010 electron microscope operating at an acceleration voltage of 120 kV. Samples were prepared by drop-coating aqueous solutions on a carbon-coated copper grid and drying. This rinsing procedure was repeated three times, and then the grid was negatively stained with uranyl acetate. SAED and EDS were obtained on the same instrument. AFM measurements were carried out in tapping mode in air on a commercial multimode Nanoscope IVAFM. Samples were prepared in the same manner as for TEM experiments. SLS measurements were performed on a commercial laser light scattering (LLS) spectrometer (ALV5000) equipped with a single avalanche photo diode detector and a cylindrical 22 mW Uniphase He-Ne laser (λ_0 = 632.8 nm). The LLS cell was held in a refractive index-matching vat filled with purified and dust-free toluene and fitted with a thermostat. DLS measurements were performed on a Malvern ZS 90 Zetasizer instrument. Single crystal XRD data was collected on an Oxford Gemini E diffractometer, and XRD data were recorded on a Rigaku D/max 2500 diffractometer. The Bragg peak was extracted from the XRD data and the layer thickness *d* was obtained using the Bragg equation $d = \lambda/2\sin\theta$, $\lambda = 1.15405$ nm. The sample was prepared by dropwise addition of the solution onto a clean silicon substrate at room temperature.

1. Synthesis of compound PAL

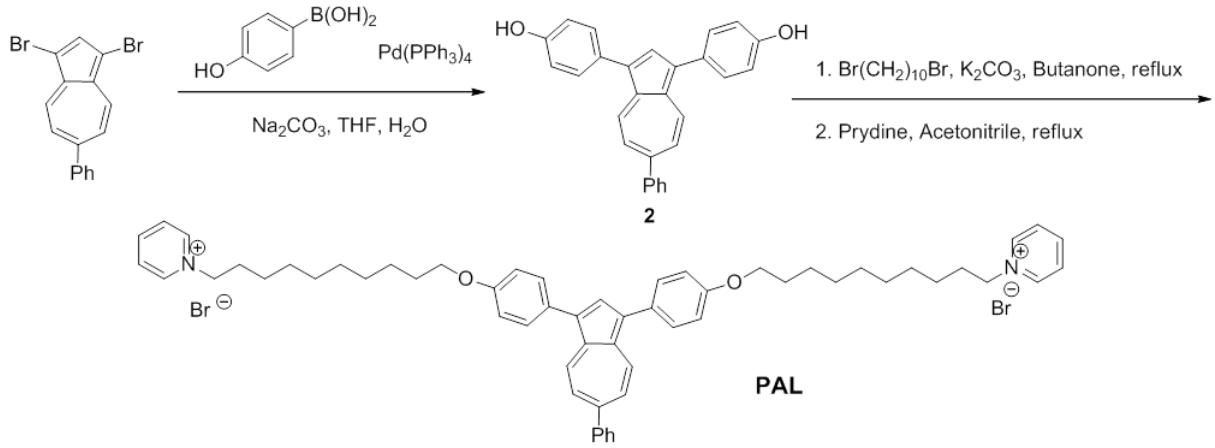

Scheme S1. Synthesis of PAL

The synthetic route of PAL is shown in Scheme S1. Compound **2**[1]: A mixture of 1,3-dibromo-6-phenylazulene (340 mg, 0.94 mmol), (4-hydroxyphenyl)boronate pinacol ester (620 mg, 2.82 mmol), Na_2CO_3 (996 mg, 9.4 mmol), and [$Pd(PPh_3)_4$] (108 mg, 1.135 g) in THF (20 mL, freshly distilled) and water (6 mL) was stirred and refluxed overnight under N_2 atmosphere. The mixture was added with water (100 mL) and extracted with ethyl acetate. The combined organic phase was dried over Na_2SO_4 and concentrated in vacuo. The residue was purified by flash chromatography (petroleum ether/ ethyl acetate: 4/1 to 2/1) to afford product **2** as a green solid (345 mg, 94% yield). ^{1}H NMR ($CDCl_3$, 300 MHz): δ = 8.48 (d, J = 10.2 Hz, 2H), 7.99 (s, 1 H), 7.80 – 7.13 (m, 11 H), 7.11 -6.93 (m, 4 H), 5.17 (s, 2H).

PAL: A mixture of compound **2** (345 mg, 0.89 mmol), 1,10-dibromodecane (2.7 g, 9 mmol) and K_2CO_3 (2.7 g, 19.5 mmol) in butanone (20 mL) was stirred and refluxed in two days. The mixture was concentrated in vacuum, then added with water (50 mL) and extracted with ethyl acetate (50 mL × 3). The combined organic phase was consequently washed with water and brine, and dried over Na_2SO_4. The concentrated residue was purified by flash chromatography (petroleum ether/ ethyl acetate: 50/1 to 25/1 to 10/1) to afford the intermediate as a green crystal. To the solution of intermediate in acetonitrile (10 mL) was added pyridine (10 mL). The resulting mixture was stirred and refluxed for three days under N_2 atmosphere. The solvent was removed in vacuum. The residue dissolved in mixed solvent (CH_2Cl_2/MeOH = 1/1, 1 mL) was added dropwise into diethyl ether (100 mL). The solid precipitation was filtered and dried to give PAL (302 mg, 35% yield) as a green solid. ^{1}H NMR (CD_3OD, 600 MHz) δ 9.02 (d, J = 5.4 Hz, 4H), 8.60 (m, 2H), 8.49 (d, J = 10.7 Hz, 2H), 8.12 (t, J = 7.1 Hz, 4H), 7.98 (s, 1H), 7.70 (m, 2H), 7.59 – 7.53 (m, 4H), 7.53 – 7.47 (m, 2H), 7.47 – 7.42 (m, 1H), 7.31 (d, J = 10.7 Hz, 2H), 7.10 – 7.03 (m, 4H), 4.65 (dd, J = 18.2, 10.6 Hz, 4H), 4.06 (t, 4H), 2.10 – 1.96 (m, 4H), 1.89 – 1.75 (m, 4H), 1.60 – 1.48 (m, 4H), 1.47 – 1.28 (m, 20H); ^{13}C NMR (CD_3OD, 150 MHz) δ 138.3, 128.1, 127.7, 127.4, 120.6, 119.7, 119.6, 116.2, 116.1, 115.9, 115.3, 114.6, 114.2, 114.1, 114.1, 110.1, 103.4, 65.9, 61.1, 36.7, 35.1, 35.0, 35.00, 34.7, 32.4, 32.4; ESI-MS (*m/z*): 412.6 (M^{2+}).

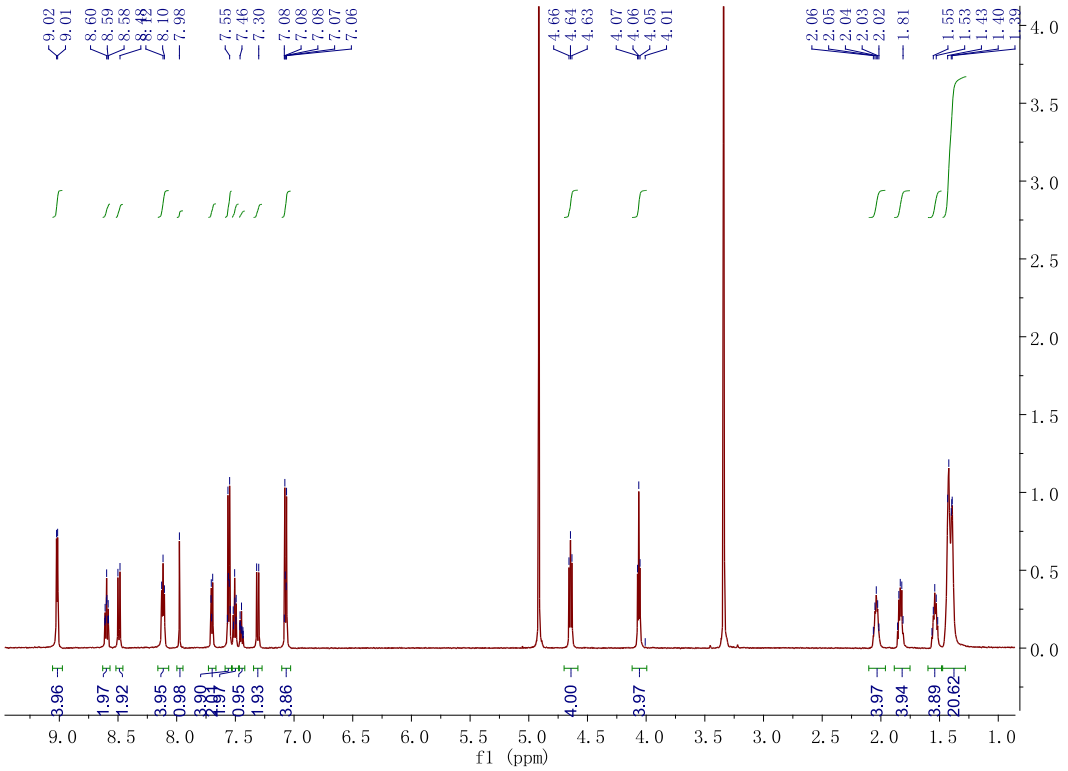

Figure S1. ^{1}H NMR spectrum of PAL

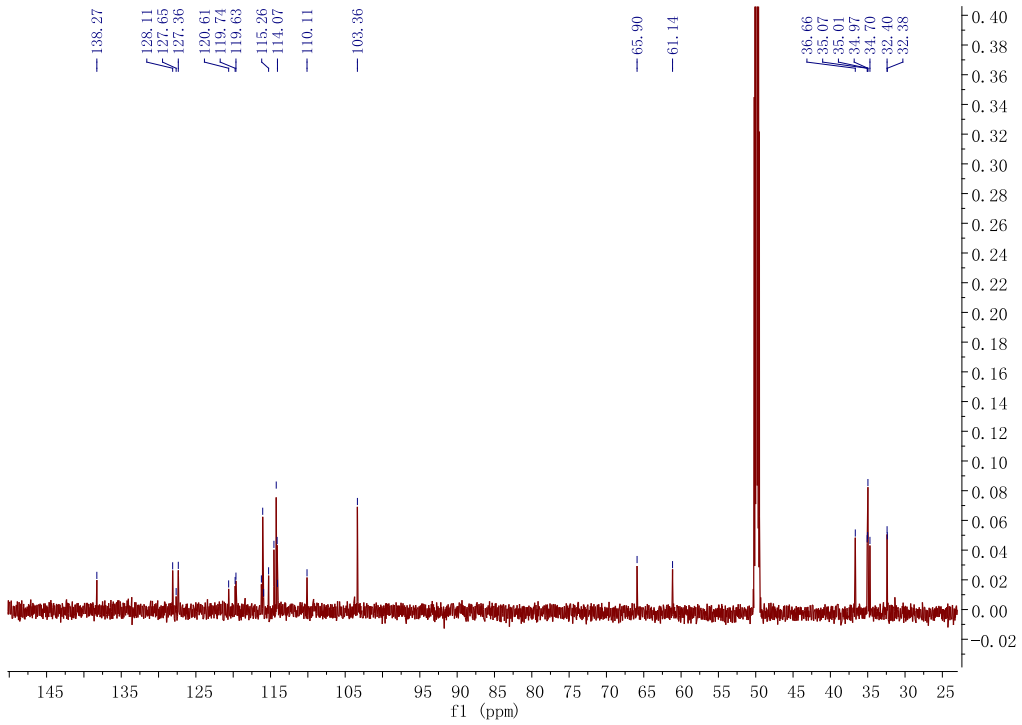

Figure S2. ^{13}C NMR spectrum of PAL

2. Self-assembly of PAL

UV/Vis absorption and emission spectra of PAL in H_2O (Figure S3a) and MeOH (Figure S3b). As shown in Figure S3, compared with that of PAL in methanol, the absorption of PAL in water greatly decreased, and the emission is significantly quenched, indicating that the PAL self-assembles in aqueous media.

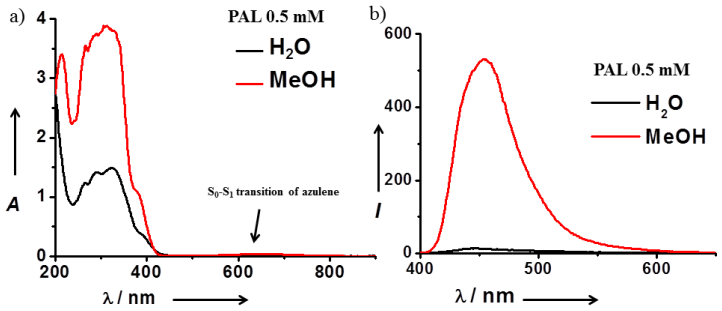

Figure S3. a) UV/Vis absorption spectra of PAL in H_2O and MeOH; b) Fluorescent spectra of PAL in H_2O and MeOH (EM slit: 10 nm, EX silt: 10 nm). The concentration of PAL in the experiments was 5×10^{-4} M.

3. Self-assembly of PAL-pyrene complexes

3.1. Systematic temperature-dependent UV/Vis experiments were carried out to provide evidence of CT complexation and identify the absorption caused by hetero-association between PAL and pyrene (Figure S4).

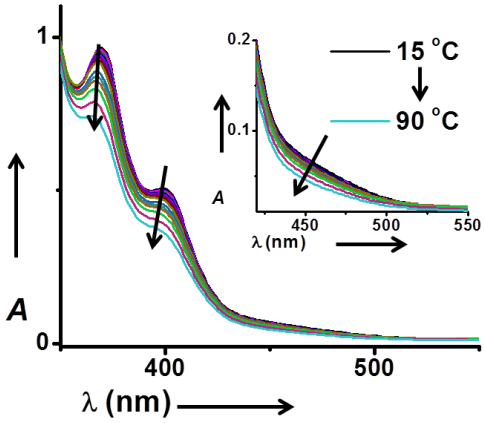

Figure S4. Temperature–dependent UV/Vis spectra of complex solution at intervals of 5 °C.

3.2. UV/Vis experiments were carried out to prove that addition of ethyl ether could extract pyrene out of the PAL-pyrene aqueous solution (Figure S5).

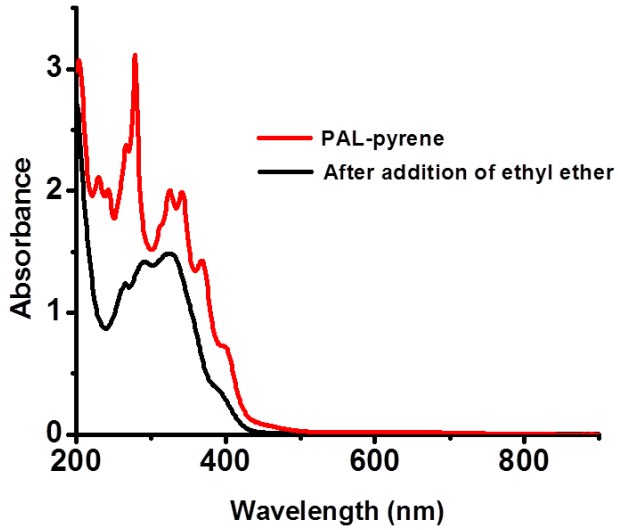

Figure S5. UV/Vis absorption spectra of PAL-pyrene aqueous solution (0.5 mM) and after extraction of pyrene out of the solution.

3.3. The UV/Vis spectra were obtained by adding different molar ratio of pyrene into PAL solution (Figure S3). As exhibited, there is no change of the CT absorptions as the molar ratio of pyrene/ PAL is above 1 to 1.

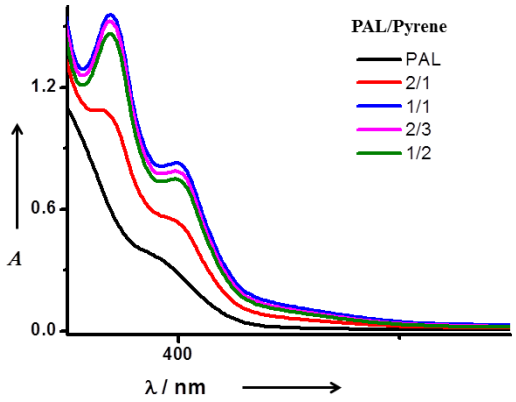

Figure S6. UV/Vis spectra of PAL (0.5 mM) upon addition of different molar ratio of pyrene (20 mM). The resulting solution was deposited in 36 hours.

3.4 DLS data showed that the average aggregate sizes increased significantly from 116 to 322 nm upon initial addition of pyrene into the PAL solution, and then decreased to 168 nm after complete CT complexation (Figure S7).

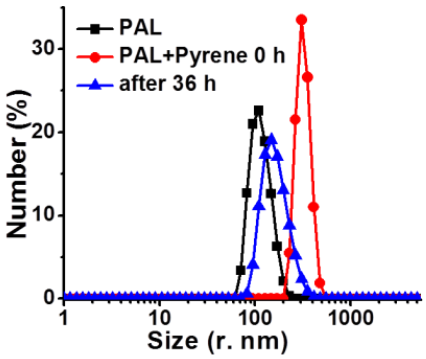

Figure S7. Size distributions of PAL solution, immediately after mixing of PAL and pyrene, and the same solution after 36 h obtained from DLS experiments. The concentration of PAL solution 1×10^{-4} M; The concentration of pyrene in THF was 2×10^{-2} M.

3.5 The UV/Vis and emission spectra were obtained by monitoring the process of adding pyrene (20 mM in THF) into PAL aqueous solution (Figure S8). The absorption of pyrene gradually appeared and the emission of pyrene excimer gradually quenched in the CT complexation.

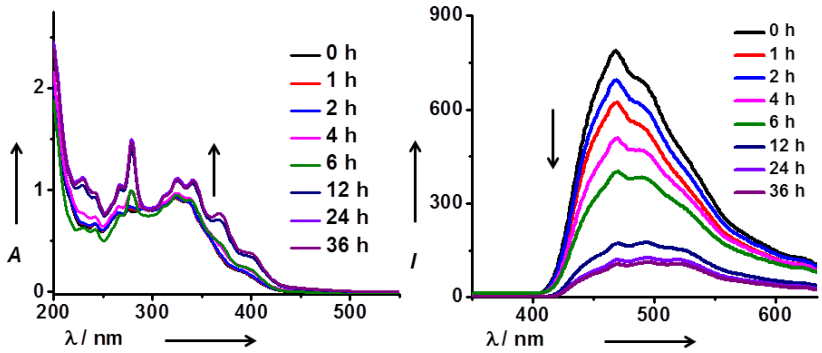

Figure S8. a) Time-resolved UV/Vis absorption spectra of complex solution; b) Time-resolved emission spectra of complex solution with excitation wavelength of 335 nm;

3.6 The self-assembly behavior of the CT complexes were investigated by higher dilution experiment. It showed the strong emission of pyrene monomers appeared when the concentration is below 0.1 mM, confirming that PAL and pyrene associated above that concentration (Figure S9).

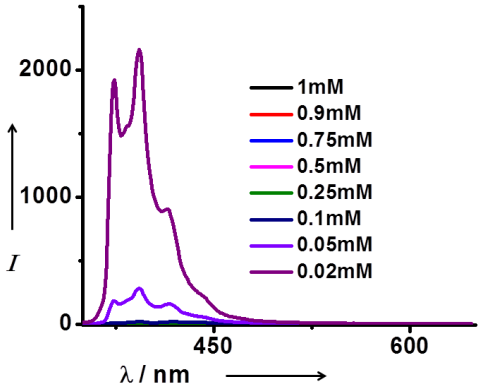

Figure S9. Emission spectra of PAL-pyrene assembly on dilution with excitation at the wavelength 335 nm.

3.7 Selected area electron diffraction pattern of PAL-pyrene complexes was obtained by exposing multiple-layered stacking nanosheets to the strong electron beam (Figure S10). It displayed two Debye-Scherrer ring patterns around the discrete diffraction spots, indicating the crystalline order inside the PAL-pyrene assemblies. The outer ring corresponds to a distance of 0.39 nm, which can be associated with the π-π stacking distance between PAL and pyrene. The inner ring corresponds to a distance of 0.44 nm, which can be associated with the characteristic of the average spacing of molecules between PAL and pyrene.

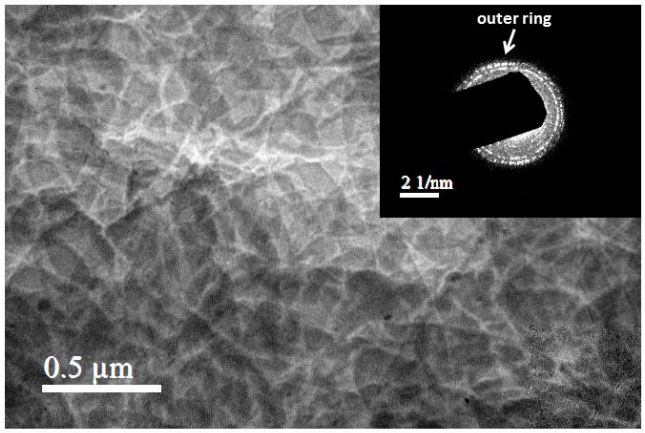

Figure S10. Selected area electron diffraction pattern of PAL-pyrene complexes

4. Structure elucidation of PAL-pyrene complexes

Small angel X-ray diffraction (SAXD) experiments were carried out to determine the existence of the layered structure of PAL and PAL-pyrene complexes on the nanoscale. The results demonstrate that PAL possesses a lamellar structure in the bulk state and PAL-pyrene complexes give no such structure information as dispersive single-layered disklike nanosheets (Figure S11).

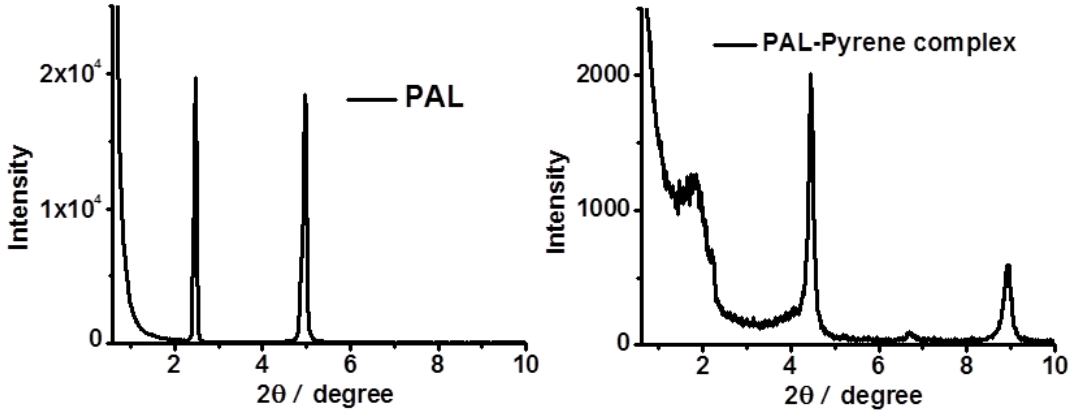

Figure S11. SAXD pattern of self-assemblies of a) PAL; and b) PAL-pyrene complexes.

5. Single crystal structure of BPA.

As exhibited in Figure S12, the single crystal of 1, 3-bis(4-butoxyphenyl)-6-phenylazulene (BPA) was obtained by evaporating its hexane/THF solution (v/v = 1:1). Crystallographic data for BPA (C36H36O2): T = 131.4 K; wavelength: 0.71073 Å; crystal system: triclinic; space group: P-1; unit cell dimensions: a = 7.5304 (11) Å, b = 14.758 (2) Å, c = 25.121 (3) Å, α = 86.245 (12)˚, β = 89.150 (11)˚, γ = 77.402 (14)˚; V = 2718.7 (7) Å3; Z = 4;

ρcalc = 1.223 mg mm-3; F(000) = 1072; final R indices [I > 2σ (I)]: R1 = 0.0696, wR2 = 0.1617; R indices (all data), R1 = 0.0953, wR2 = 0.1759; 19663 reflections collected, 10663 were unique (R(int) = 0.0357 (inf – 0.9 Å)). CCDC-889453 (BPA) contains the supplementary crystallographic data (and details of the data handling and structure refinement) for this paper. These data can be obtained free of charge from the Cambridge Crystallographic Data Centre via www.ccdc.cam.ac.uk/data_request/cif.

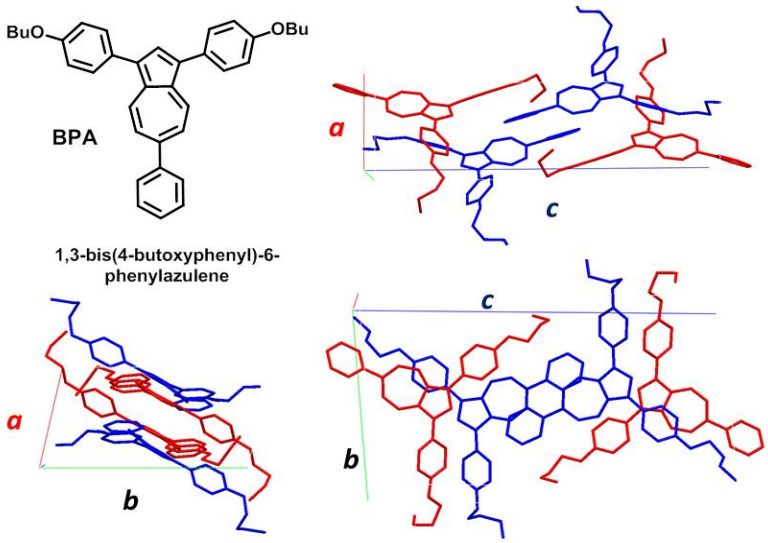

Figure S12. Single crystal images of BPA representing the cell lattice with three axes. Molecular skeletons of the same color possess equivalent symmetry. Hydrogen atoms were omitted for clarity.

6. Explanation why PAL self-assemblies show cylindrical micelles with negative staining (1.5 wt% uranyl acetate) in the TEM images.

We had proved that the PAL self-assemblies are cylindrical micelles in aqueous solution by SLS experiments (Figure 2b) and show a layered structure in the solid state by SAXD experiments (Figure S11a). However, the TEM images of PAL self-assemblies which were stained with uranyl acetate showed cylindrical micelles in the solid state. That is very interesting and we have done a series of experiments to explain this phenomenon. At first, we have used PAL aqueous solutions with different concentrations from 2 mM to 0.5 mM to prepare the TEM samples. All of the samples were prepared by the following method. 10 μL of the sample solution was applied to a carbon-coted copper grid for 5 min × 2. After removal of excess solution with filter paper, the grid was negatively stained with 10 μL of 1.5% (w/w) uranyl acetate aqueous solution for 45 seconds × 2. The excess solution was removed by filter paper. The resultant grid was dried in the air for at least 2 hours. All of the samples showed cylindrical micelles in their TEM images (Figure S13). However, we could not obtain such cylindrical micelles without negative staining of uranyl acetate anyway, because PAL assemblies show lamellar structures in the solid state. It seemed that aqueous uranyl acetate solution had led to such the morphology transformation of PAL self-assemblies.

Further experiments were carried out to illustrate the process. We dropped 10 μL of PAL aqueous solution (8 mM) to a carbon-coted copper grid for 5 min, then removed the solution and dried the resultant grid for 12 hours. The TEM images were obtained with miceller aggregates that may index to a lamellar structure which was proved by SAXD experiments (Figure S14a and Figure S14b). After TEM observation, the neat PAL sample was stained with 1.5% (w/w) uranyl acetate aqueous solution for 45s, then removed the excess solution by filter paper and dried the sample for 12 hours. As shown in Figure S14c and Figure S14d, the cylindrical micelles appeared with a periphery which was similar to that of unstained PAL samples. The water could drive the neat micelles with lamellar structures to form cylindrical micelles in aqueous solution on the surface, but we were still wondering how the cylindrical micelles could be fixed on the base without recover to the lamellar structures on the drying process. Furthermore, we

observed both of lattice spots and stripes in the spacings between two adjacent cylindrical micelles on the High Resolution Transmission Electron Microscopy (HRTEM) images (Figure S15a). Use of Fourier transformation on calculation of the lattice plane affords the spacings with a = b = 0.30 nm and c = 0.34 nm, which corresponds to the lattice *d*-spacings of uranyl acetate (Figure S16). Energy Dispersive Spectroscopy (EDS) experiments evidenced the existence of uranyl acetate in the area of cylindrical micelles but non-existence of uranyl acetate in the blank space (Figure S17). Consequently, a reasonable mechanism could be given. In the short staining process (45 seconds), water drove the PAL miceller structures in the solid state to form cylindrical miceller structures on the surface of the solid, then residual uranyl acetate played a role to fix the cylindrical micelles by crystallization in the spacings of them after removal of the solution. Therefore, the cylindrical micelles were preserved after drying process with negative staining of uranyl acetate (Scheme S2).

6.1. TEM images of samples prepare by different PAL solutions with different concentrations from 2 mM to 0.5 mM (Figure S13).

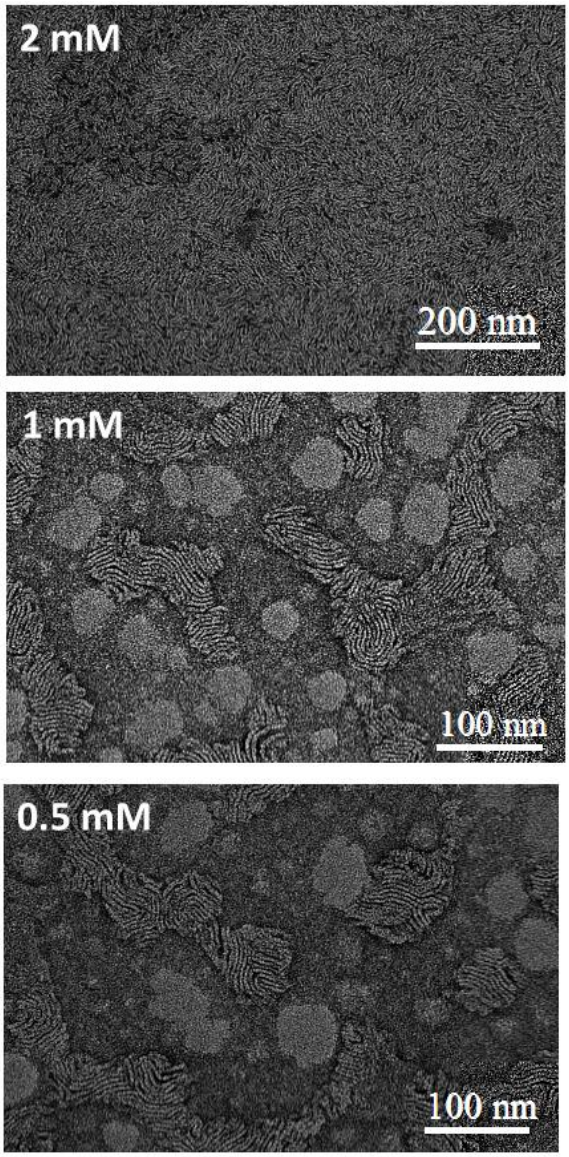

Figure S13. TEM images of PAL self-assemblies with negative staining (1.5 wt% uranyl acetate) in different concentrations (2 mM, 1 mM and 0.5 mM)

6.2. TEM experiments were carried out to compare the PAL self-assemblies before and after negative staining with the uranyl acetate (1.5 wt% aqueous solution) (Figure S14). It should be noted that both of the samples were prepared under drying process in the air.

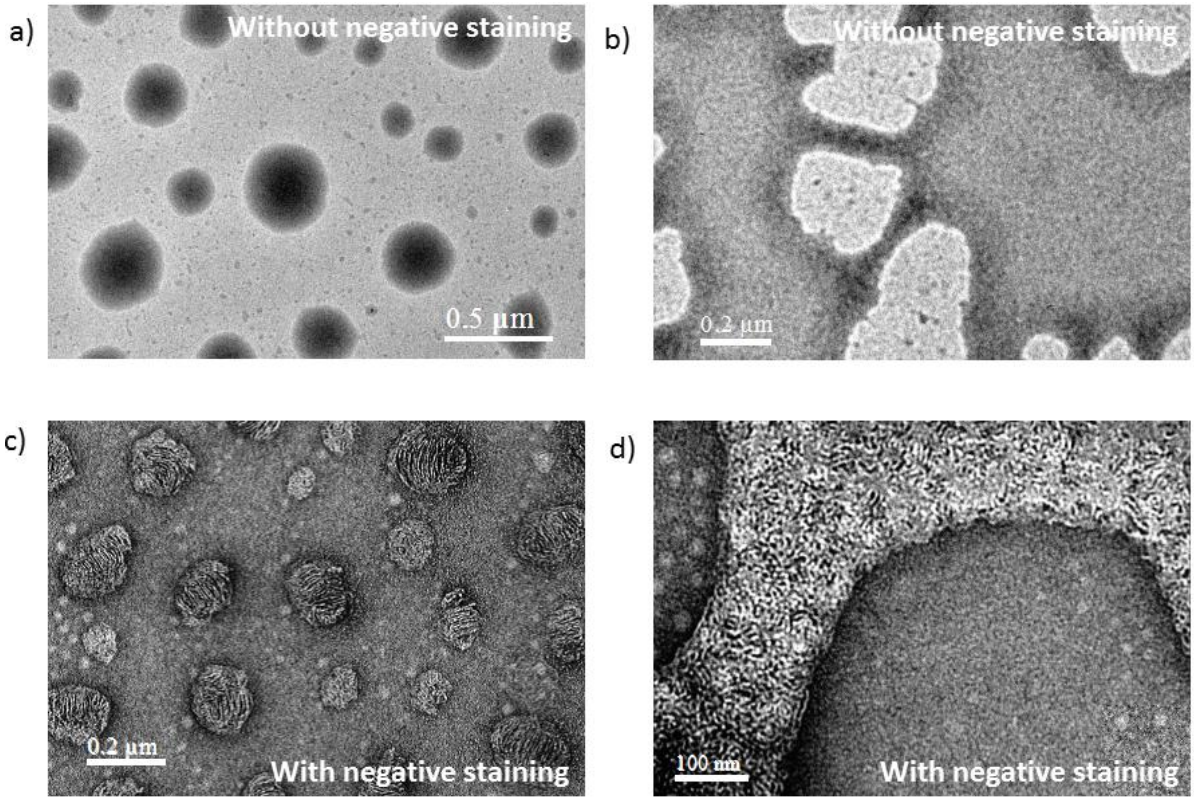

Figure S14. a) and b) TEM images of PAL assembly without staining; c) and d) TEM images of PAL assembly with negative staining using the uranyl acetate (1.5 wt % aqueous solution).

6.3. We had observed both of spots and stripes in the spacings of cylindrical micelles in the HRTEM experiments. The diffraction patterns were calculated by Fourier transformation with lattice spacings: a = b = 0.30 nm and c = 0.34 nm (Figure S15).

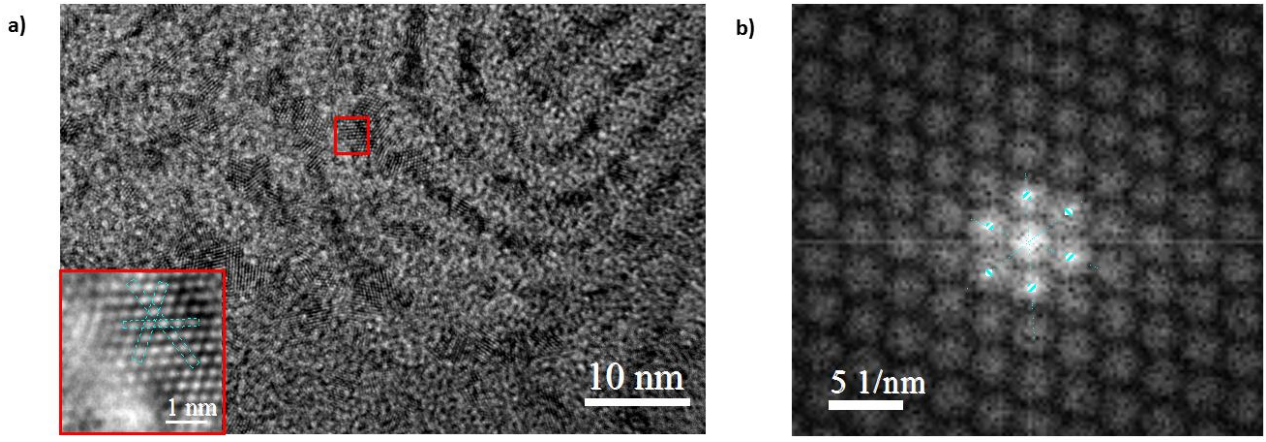

Figure S15. a) HRTEM lattice images of self-assemblies of PAL with negative staining using uranyl acetate (1.5 wt % aqueous solution); b) Diffraction pattern by Fourier transformation with application of mask on calculation of the lattice plane spacings: a = b = 0.30 nm, c = 0.34 nm.

6.4. XRD pattern of an uranyl acetate sample were obtained for comparison (Figure S16). The sample were prepared by drop of uranyl acetate solution on the glass and drying in the air.

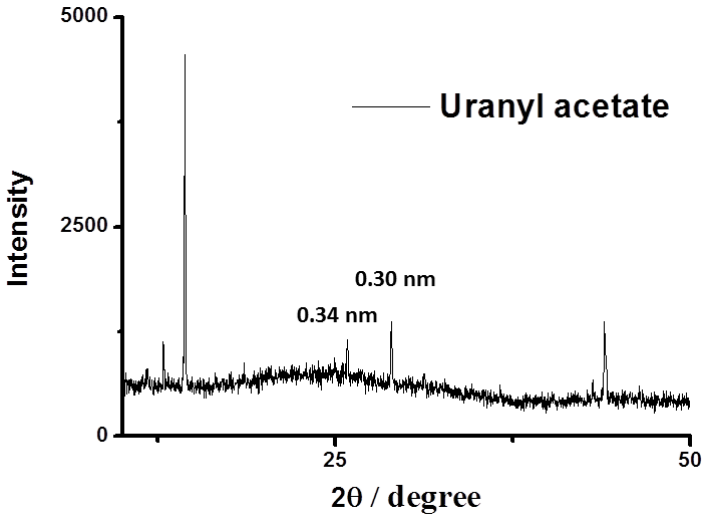

Figure S16. XRD pattern of uranyl acetate.

6.5. EDS experiments were measured to provide evidence that the PAL self-assemblies with negative staining contain uranyl acetate (Figure S17)

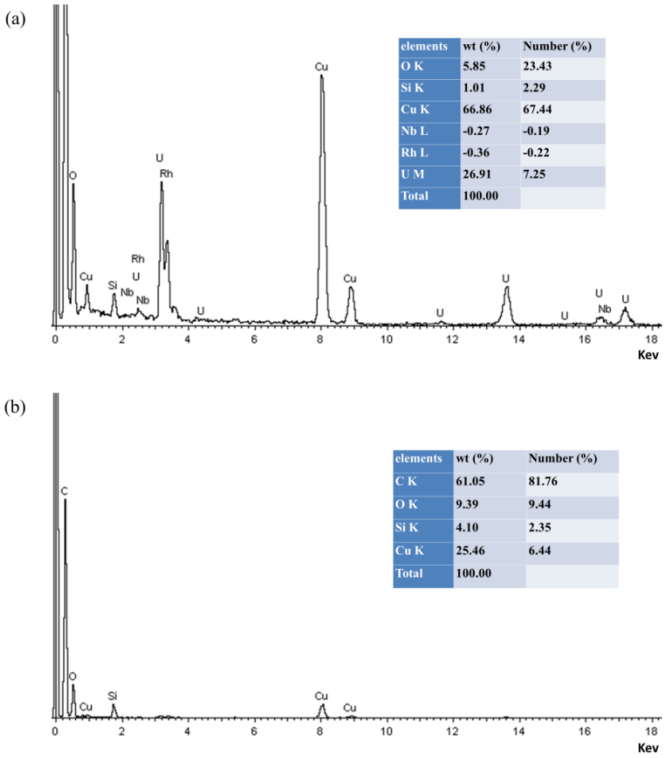

Figure S17. EDS data of PAL self-assemblies with with negative staining using uranyl acetate (1.5 wt % aqueous solution): a) in the area of cylindrical micelles and b) in the blank space.

6.6. Schematic representation of the process: water drive the PAL self-assemblies with lamellar structures in the bulk state to form cylindrical micelles after exposure of water on its surface, and after removal of the solution, the residual uranyl acetate crystallize in the spacings of the cylindrical micelles to fix such morphology in the period of drying process (Scheme 2)

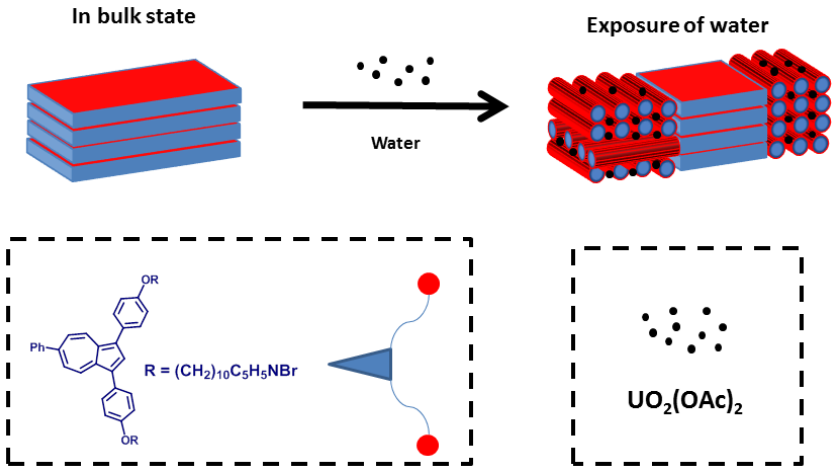

Scheme 2 Schematic representation of the generation of the cylindrical micelles of PAL self-assemblies on TEM images.

[1] T. D. Lash, J. A. El-Beck, G. M. Ferrence, *J. Org. Chem.* **2007**, *72*, 8402-8415.